Biological sciences; biophysics and computational biology

Consensus sequence design as a general strategy to create hyperstable, biologically active proteins

Matt Sternke[1], Katherine W. Tripp[1], & Doug Barrick[1]*

[1]The T.C. Jenkins Department of Biophysics, Johns Hopkins University, 3400 N. Charles St., Baltimore, MD 21218 USA.

*To whom correspondence should be addressed.

Email addresses: msternk1@jhu.edu, tripp@jhu.edu, and barrick@jhu.edu

Keywords: consensus sequence design, protein stability, protein function

Abstract

Consensus sequence design offers a promising strategy for designing proteins of high stability while retaining biological activity since it draws upon an evolutionary history in which residues important for both stability and function are likely to be conserved. Although there have been several reports of successful consensus design of individual targets, it is unclear from these anecdotal studies how often this approach succeeds, and how often it fails. Here, we attempt to assess the generality of consensus by designing consensus sequences for a set of six protein families over a range of chain-lengths, structures, and activities. We characterize the resulting consensus proteins for stability, structure, and biological activities in an unbiased way. We find that all six consensus proteins adopt cooperatively folded structures in solution. Strikingly, four out of six of these consensus proteins show increased thermodynamic stability over naturally-occurring homologues. Each consensus proteins tested for function maintained at least partial biological activity. Though peptide binding affinity by a consensus-designed SH3 is rather low, K_m values for consensus enzymes are similar to values from extant homologues. Moreover, steady-state turnover rates are on par with values for thermophilic proteins. An analysis of sequence properties of consensus proteins shows these proteins to be enriched in charged residues, and rarified in uncharged polar residues. Sequence differences between consensus and extant homologues are predominantly located at weakly conserved surface residues, highlighting the importance of these residues in the success of the consensus strategy in generating folded and functional proteins of high stability.

Significance Statement

A major goal of protein design is to create proteins that have high stability and biological activity. Drawing on evolutionary information encoded within extant protein sequences, consensus sequence design has produced several successes in achieving this goal. Here we explore the generality with which consensus design can be used to enhance protein stability and maintain biological activity. By designing and characterizing consensus sequences for six unrelated protein families, we find that consensus design shows high success rates in creating well-folded, hyperstable proteins that retain biological activities. Remarkably, many of these consensus proteins show higher stabilities than naturally-occurring sequences of their respective protein families. Our study highlights the utility of consensus sequence design and informs the mechanisms by which it works.

Introduction

Exploiting the fundamental roles of proteins in biological signaling, catalysis, and mechanics, protein design offers a promising route to create and optimize biomolecules for medical, industrial, and biotechnological purposes (1–3). Many different strategies have been applied to designing proteins, including physics-based (4), structure-based (5, 6), and directed evolution-based approaches (7). While these strategies have generated proteins with high stability, implementation of the design strategies is often complex and success rates can be low (8–11). Though directed evolution can be functionally directed, *de novo* design strategies typically focus primarily on structure. Introducing specific activity into *de novo* designed proteins is a significant challenge (8, 10).

Another strategy that has shown success in increasing thermodynamic stability of natural protein folds is consensus sequence design (12). For this design strategy, "consensus" residues are identified as the residues with the highest frequency at individual positions in a multiple sequence alignment (MSA) of extant sequences from a given protein family. The consensus strategy draws upon the hundreds of millions of years of sequence evolution by random mutation and natural selection that is encoded within the extant sequence distribution, with the idea that the relative frequencies of residues at a given position reflect the "relative importance" of each residue at that position for some biological attribute. As long as the importance at each position is largely independent of residues at other positions, a consensus residue at a given

position should optimize stability, activity, and/or other properties that allow the protein to function in its biological context and ultimately contribute to organismal fitness[†]. By averaging over many sequences that share similar structure and function, the consensus design approach has the potential to produce proteins with high levels of thermodynamic stability and biological activity, since both attributes are likely to lead to residue conservation.

There are two experimental approaches that have been used to examine the effectiveness of consensus information in protein design: point-substitution and "wholesale" substitution. In the first approach, single residues in a well-behaved protein that differ from the consensus are substituted with the consensus residue (13–17). In these studies, about half of the consensus point substitutions examined are stabilizing, but the other half are destabilizing. Although this frequency of stabilizing mutations is significantly higher than an estimated frequency around one in 10^3 for random mutations (13, 18, 19), it suggests that combining individual consensus mutations would give minimal net increase in stability since stabilizing substitutions would be offset by destabilizing substitutions.

The "wholesale" approach does just this, combining all substitutions toward consensus into a single consensus polypeptide composed of the most frequent amino acid at each position in sequence. The stabilities of several globular proteins and several repeat proteins have been increased using this approach (20–29). An increase in thermodynamic stability is seen in most (but not all) cases, but effects on biological

[†] These properties include rates of folding, unfolding, degradation, compartmentalization, oligomerization, and solubility.

activity are variable. In a recent study, our lab characterized a consensus-designed homeodomain sequence that showed a large increase in both thermodynamic stability and DNA-binding affinity (30). Unlike the point-substitution approach, where both stabilizing and destabilizing substitutions are reported, the success rate of the wholesale approach is not easy to determine from the literature, where publications present single cases of success, whereas failures are not likely to be published. One study of TIM barrels reported a few poorly behaved consensus designs that were then optimized to generate a folded, active protein (22). Although this study highlighted some limitations, it would not likely have been published if it did not end with success.

Here, we address these issues by applying the consensus sequence design strategy to a set of six taxonomically diverse protein families with different folds and functions (Figure 1). We chose the three single domain families including the N-terminal domain of ribosomal protein L9 (NTL9), the SH3 domain, and the SH2 domain, and the three multi-domain protein families including dihydrofolate reductase (DHFR), adenylate kinase (AK), and phosphoglycerate kinase (PGK). We characterized these six consensus proteins in terms of structure, stability, and function. We find that consensus sequences for all six protein families are quite soluble, and adopt the native folds of their respective families. Strikingly, four of the six consensus proteins show increased thermodynamic stability compared to naturally-occurring homologues; the other two consensus proteins show stabilities comparable to natural homologues. All consensus proteins assayed for biological activity retain their expected activities, including molecular recognition and enzymatic catalysis. An advantage of this multi-target

comparison is that it allows us to examine sequence features of consensus-designed proteins and relate them to one another and to naturally occurring homologues. This sequence analysis shows that consensus proteins are enriched in charged residues, are depleted in polar uncharged residues, and highlights the importance of weakly conserved surface residues in enhancing stability through the consensus design strategy.

Results

Consensus sequence generation

The six families targeted for consensus design are shown in Figure 1. To generate and refine multiple sequence alignments from these families, we surveyed the Pfam (31), SMART (32), and InterPro (33) databases to obtain sets of aligned sequences for each family. For each family, we used the sequence set that maximized both the number of sequences and quality of the multiple sequence alignment (Table S1). For five of the six protein families, we did not limit sequences using any structural or phylogenetic information. For AK, we selected sequences that contained a "long type" LID domain containing a 27-residue insertion found primarily in bacterial sequences (34). The number of sequences in these initial sequence sets ranged from around 2,000 up to 55,000 (Table S1).

To improve alignments and limit bias from copies of identical (or nearly identical) sequences, we removed sequences that deviated significantly (±30%) in length from the median length value, and removed sequences that shared greater than 90% sequence

identity with another sequence. This curation reduced the size of sequence sets by an average of 65% (ranging from 30% to 80%; Table S1). Final sequence sets ranged from 1,355 (NTL9) to 14,474 (SH3) sequences, and showed broad ranges of sequence variability (quantified by average pairwise identities among sequences in the set) and phylogenetic distribution (Table S1).

Curated sequence sets were aligned, and consensus sequences were determined from the most probable residue at each position (Table S2). Consensus sequences differ substantially from aligned sequences from which they are derived. The maximum identity between consensus sequences and the most similar extant sequence in the corresponding alignment ranges from 63% for SH2 to 80% for NTL9; the average pairwise identity between consensus sequences and each sequence in the corresponding alignment ranges from 58% for NTL9 and PGK to 40% for SH3 and SH2 (Figure S2).

Structural characterization of consensus proteins

To determine whether the six consensus sequence proteins adopt their target folds, we expressed and purified consensus proteins for each of the six protein families and characterized them using CD and NMR spectroscopies. Far-UV CD spectra for consensus NTL9, AK, and PGK show minima at 222 and/or 208 nm (Figure 2A), consistent with α-helical secondary structure. Spectra for consensus SH2 and DHFR show single minima at 219 and 214 nm respectively, consistent with predominantly β-sheet secondary structure. Consensus SH3 shows a far-UV CD spectrum with minima

at 228 and 204 nm and a maximum at 219 nm, similar to published spectra for a naturally-occurring SH3 domain (35).

With the exception of consensus DHFR, ^{1}H-^{15}N HSQC and TROSY (for PGK) NMR spectra for each consensus protein show sharp resonances that are well dispersed in the ^{1}H dimension (Figure 2B--G), indicating that these consensus proteins adopt well-folded tertiary structures. These six consensus proteins show between 88--99% of expected cross-peaks in the ^{1}H-^{15}N HSQC and TROSY (PGK) spectra, suggesting that the consensus proteins maintain rigid tertiary structure over most of their sequence. The high signal-to-noise and sharp cross-peaks indicate that these consensus proteins have high solubility at NMR concentrations (ranging from 400--800 μM).

For DHFR, the ^{1}H-^{15}N HSQC spectrum shows rather broad resonances and only around 60% of expected cross peaks (Figure S3). However, addition of the substrate analog methotrexate both sharpens resonances and increases the number of resolved cross peaks (Figure 2E), suggesting that consensus DHFR may undergo a large-scale conformational change and rigidification upon binding. This behavior has been observed in a study of two naturally-occurring DHFR proteins (36).

To determine the location of α-helices and β-strands, we assigned backbone resonances for consensus NTL9, SH3, and SH2. Using standard triple-resonance experiments, we were able to assign backbone ^{1}H and ^{15}N resonances, as well as ^{13}C $C\alpha$, $C\beta$, and C' chemical shifts, for 96%, 96%, and 89% of residues for consensus NTL9, SH3, and SH2 respectively (Figures S4--S6). Secondary chemical shift-based

secondary structure predictions using these resonances show α-helix and β-strand boundaries that largely match secondary structure locations in consensus homology models, suggesting that the consensus proteins adopt their archetypal folds (Figure 2H--J).

Equilibrium stability of consensus proteins

To determine equilibrium folding free energies, we measured guanidine hydrochloride-induced unfolding transitions for all consensus proteins using a combination of CD and fluorescence spectroscopies. All consensus proteins show sigmoidal unfolding transitions (data converted to fraction folded in Figure 3A, raw data in Figure S7), indicating that the consensus proteins unfold in a cooperative manner similar to naturally-occurring proteins. All consensus proteins were found to fold and unfold reversibly, allowing us to determine equilibrium folding free energies and *m*-values by fitting a two-state linear extrapolation model to each curve. Folding free energies ranged from -3.2 kcal/mol for consensus SH3 to -13.6 kcal/mol for consensus AK (Table 1). Measured *m*-values for consensus NTL9 and SH2 match values predicted from an empirical relationship based on chain-length (37, 38) within 5%, suggestive of two-state folding. The measured *m*-value for consensus SH3 is 30% larger than the predicted value. Measured *m-value*s for consensus DHFR, AK, and PGK are 20%, 50%, and 70% smaller than predicted values, suggesting the population of partly folded states in the folding transition region. As a result, estimated folding free energies for

these constructs are likely to underestimate the free energy difference between the native and denatured states.

To compare the measured folding free energies of the consensus proteins with extant sequences, we gathered folding free energy values from the literature for naturally-occurring sequences for each protein family. We limited our search to folding free energy values determined by chemical denaturation experiments and to proteins that appear to be monomeric[‡]. For comparison, we have included the consensus homeodomain that we recently characterized with this approach (30).

The stabilities of six of the seven consensus proteins are greater than the mean stabilities of the extant homologues (Figure 3B, Table S3), with stability increases ranging from 8.3 kcal/mol for consensus AK to 1.4 kcal/mol for consensus PGK (although for PGK, fitted $\Delta G°$ parameters are likely to underestimate the free energy difference between native and denatured ensembles since the unfolding transition is almost certainly multistate). The sole exception to this observation is consensus SH3, which shows a stability that is 0.3 kcal/mol less than the mean value for the extant homologues. Furthermore, stabilities of five of the seven consensus proteins (NTL9, HD, SH2, DHFR, and AK) are greater than that of the most stable extant homologue, ranging from 0.6 kcal/mol for consensus SH2 to 3.8 kcal/mol for consensus AK (Figure 3B, Table S3).

Characterization of consensus SH3 peptide binding

[‡] Although for most families this search resulted in five or more free energy values, providing a good representation of the average stability, all of these stabilities may be biased by experimental constraints (expression, solubility, and baseline-resolved folding transitions.

To measure binding of consensus SH3 to a target peptide, we acquired a synthetic peptide (Ac-PLPPLPRRALSVW-NH_2), which contains a proline-rich motif used in previous binding studies of the human Fyn SH3 domain, a well-studied extant sequence with peptide contact residues that match those in consensus SH3 (39, 40). ^{1}H-^{15}N HSQC spectra of ^{15}N-labelled consensus SH3 at increasing concentrations of unlabeled peptide show shifts in some (but not all) peaks (Figure S8). This behavior is consistent with formation of a complex that is in fast exchange on the chemical shift timescale. When plotted on a homology model of consensus SH3, the largest chemical shift perturbations (CSPs) cluster on the canonical peptide-binding site (Figure 4A). A global fit of a single-site binding model to the 10 residues displaying the largest CSPs gives a K_d of 795 $\pm$ 13 μM (Figure 4B; the reported uncertainty is at a 67% confidence level derived from 5000 bootstrap iterations in which residuals are randomly resampled with replacement). This measured binding affinity for consensus SH3 is approximately 5000-fold weaker than a binding affinity reported for human Fyn SH3 domain binding the same peptide sequence (39).

Steady-state kinetics of consensus enzymes

To investigate how the consensus design strategy affects enzymatic activity, we characterized steady-state kinetics of catalysis for the three consensus enzymes in our set. DHFR, AK, and PGK catalyze various chemical reactions important for cellular metabolism:

$$\text{Dihydrofolate} + \text{NADPH} \rightleftharpoons \text{Tetrahydrofolate} + \text{NADP}^{+}$$

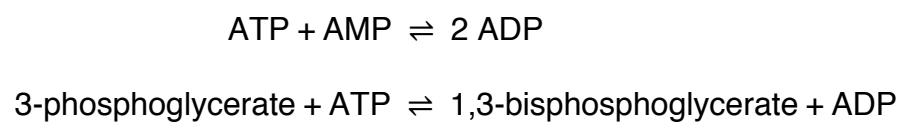

For each enzyme, we measured reaction velocities at 20 °C as a function of substrate concentration, monitoring the oxidation of NAD(P)H spectrophotometrically either as a direct read-out of activity (DHFR) or in an enzyme-coupled reaction (see Methods). Strikingly, all three consensus enzymes show substantial activity (Figure 5). Michaelis constants for the consensus enzymes are similar to those of extant enzymes, ranging from 10-fold higher to 3-fold lower than values determined under similar conditions (Table 2). Steady-state k_{cat} values determined at 20 °C for the consensus enzymes are all less than those for mesophilic homologues (Table 2), but are comparable to those for thermophilic homologues.

Sequence properties of consensus proteins and consensus mismatches

The studies above show that for all six families examined here, consensus design is successful. That is, proteins adopt well folded structures, these structures match the fold of the families from which they derived, they retain biological activity, and importantly, their stabilities equal or (more often) exceed median stabilities of extant. With this broad collection of consensus-designed proteins, we are in the position to ask whether there are any sequence features that set these consensus proteins apart from extant sequences, and if so, which features are most important for increased stability. Such properties include general features such as sequence composition, charge,

polarity, and hydrophobicity, as well as position-specific properties within each family such as degree of conservation and surface accessibility.

General sequence features. We compared various sequence properties our six consensus sequences to those of the naturally-occurring sequences within our curated multiple sequence alignments. As with the stability comparisons above, we have included a consensus homeodomain (consensus HD) that we have described previously (30). For every sequence (consensus and every sequence in each MSA), we calculated the proportion of sequence made up of charged residues, polar noncharged residues, total polar residues (the sum of charged and polar noncharged), and nonpolar residues. Similarly, we calculated the net charge of each sequence (the difference between the number of positively and negatively charged residues, assuming full positive charges for arginine and lysine, and full negative charges for aspartate and glutamate).

For each metric, the naturally-occurring sequences appeared approximately normally distributed (Figure S9). Consensus sequences show strong biases within the distributions of natural sequences for some of these sequence and structural features. Most notably, consensus sequences all lie towards the upper-tail end of the distributions for proportion of charged residues, averaging 2.1 standard deviations above the mean (Figure 6A). Conversely, consensus sequences lie toward the lower-tail end of the distributions for proportion of polar uncharged residues, averaging 2.1 standard deviations below the mean. These two biases offset in terms of total polar (charged and uncharged) residues: consensus sequences lie near the middle of the distribution for

the proportion of total polar residues, averaging 0.1 standard deviations below the mean. Likewise, consensus sequences lie near the middle of the distribution for the proportion of nonpolar residues, as would be expected given the proportion of total polar residues. Thus, it appears that the consensus design strategy implicitly creates sequences that are preferentially enhanced in charged residues at the expense of polar uncharged residues, without a large perturbation of the number of polar versus nonpolar residues. Two protein families, SH3 domain and homeodomain, deviate from this trend, however, both showing and an increase in total polar residue content and a decrease in nonpolar residue content. The net charge of five of the six consensus protein sequences are also close to mean values from the MSA for six of the seven consensus proteins, with DHFR showing the only significant deviation.

Position-specific sequence features. In addition to the general sequence features described above, which average over each sequence, we also examined the features of sequence substitution in a position-specific way. At each position in the MSA, we compared the residue of each extant sequence to the consensus residue at that position. We separated these residue-specific comparisons into “consensus matches” and “consensus mismatches” for the positions at which extant residue matched or differed from the consensus residue, respectively. Clearly, all changes in structure, stability, and function in consensus constructs compared to extant homologues result from the residues that differ from the consensus. Thus, the properties of these "consensus mismatches" are important for understanding, for

example, the increase in stability we have observed for most of our consensus constructs.

On average, there will be more consensus mismatches at positions with low sequence conservation, although there will also be some number of mismatches at positions with high conservation. One simple question that can be asked about consensus mismatches is "how biased are consensus mismatches towards positions of low conservation?" To quantify the extent to which consensus mismatches are made at sites with high conservation, we calculated the sequence entropy (41) at each position *i* in each MSA using the formula

$$S_{seq,i} = -\sum_{j \in \{20\ AA\}} p_j \ln p_j \tag{1}$$

and plotted this distribution for each family (purple distributions, Figures 6B, S10). We then weighted this distribution by the fraction of sequences in the multiple sequence alignment that differ from the consensus at each position

$$S_{mismatch,i} = p_{mismatch,i} \times S_{seq,i} \tag{2}$$

(red distributions, Figures 6B, S10) and the fraction that match the consensus at each position

$$S_{match,i} = p_{match,i} \times S_{seq,i} \tag{3}$$

(blue distributions, Figures 6B, S10).

As expected, we see a bias of consensus matches towards low sequence entropy positions and a bias of consensus substitutions towards high entropy positions. For example, at positions that have entropies below 0.5, nearly all sequences in the MSA match the consensus. Likewise, at positions that have entropies above value of 2, most sequences in the MSA differ from consensus. However, at positions with intermediate entropies (ranging from 1 to 1.5), there are significant numbers of sequences in each MSA that differ from consensus. It is possible that these substitutions disproportionately contribute to the observed stability increase of consensus proteins.

Finally, we examined the extent to which these sequence differences occur at surface positions. Since surface positions tend to be highly variable, we expect most consensus substitutions to occur at surface sites. However, since surface residues tend to contribute less to overall stability than buried residues (42, 43), we might expect the stability increases of consensus proteins to have their origins in substitutions at buried positions. To identify surface positions within each multiple sequence alignment, we generated a homology model from the corresponding consensus sequence, calculated the side chain solvent accessible surface area at each position, and referenced to the average side chain solvent accessible surface area of the same residue in an extended peptide (see Supplementary Methods). Positions (both in the consensus homology model and in all aligned sequences) were considered surface, intermediate, and buried if side chains in the homology model showed greater than 50%, 20% to 50%, and less than 20% solvent accessibility relative to the extended reference value.

A comparison of the distribution of consensus mismatches occurring at surface, intermediate, and buried positions shows that for six of the seven proteins, consensus mismatches occur most frequently at surface positions (Figure S11, darker bars). Overall, mismatches occur at surface, intermediate, and buried positions with median proportion of 0.49, 0.27, and 0.22 respectively . However, these proportions are dependent on the overall proportions of surface, intermediate, and buried residues that make up each protein. The four smaller domain families of NTL9, SH3, HD, and SH2 all have more surface residues than intermediate or buried residues (Figure S11, lighter bars). However, the larger proteins DHFR, AK, and PGK have more buried residues than surface or intermediate residues (consistent with a decreased surface to volume ratio for larger proteins).

To account for this underlying difference in surface accessibility, we divided the conditional probabilities that consensus mismatches are located at surface, intermediate, and buried positions (i.e., p(X | mismatch), where X represents the three structural classes; dark bars in Figure S11) by the overall marginal probabilities of the three structural classes (surface, intermediate, buried; light bars, Figure S11). By Bayes' theorem, this ratio represents the true enrichment (or supression) of consensus mismatches at surface, intermediate, and exposed sites. This ratio shows an enrichment of consensus mismatches at surface positions for all seven protein families (Figure 6C), with an average factor of 1.21. In contrast, there is a suppression of consensus mismatches at core positions in all seven protein families, with an average

factor of 0.71. At intermediate positions, mismatches are neither enhanced nor supressed (Figure 6C, with an average factor of 1.03).

Discussion

There are a number of reports in the literature in which consensus design has successfully been used to produce proteins that adopt their archetypical fold. This approach has found recent success for linear repeat-protein targets (44–47), but has also shown some success for globular protein targets (13, 14, 21, 24, 25). In most reports, globular consensus proteins have enhanced equilibrium stability, and sometimes retain biological activity. However, point-substitution studies suggest stability gains from wholesale consensus substitution may be marginal, and protein engineering studies with a WW domain suggest that consensus proteins may lack the coupling energies needed to fold (48). Because publications of successful design of globular proteins have so far been “one target at a time”, and since unsuccessful designs are unlikely to be published, it is difficult to estimate how likely the consensus approach is to yield folded proteins, and to determine how to improve on the approach when it performs poorly. The studies presented here, where we generate and characterize consensus sequences for six protein families, provide an unbiased look at rates of success and failure. Comparisons for different targets are aided by the use of a common design protocol for all targets, a common purification pipeline, and a uniform set of protocols for measuring stability, structure, and function. This multi-target approach also allows us to evaluate sequence features that are likely to contribute

consensus stabilization in general way, and correlate these features with measured biochemical properties.

Our results show that consensus sequence design is both a general and successful strategy for small and large globular proteins with diverse folds. For all six protein families targeted, the resulting consensus proteins expressed to high levels, remained soluble in solution, and adopted a well-folded tertiary structure. Structural information obtained from CD and NMR spectroscopies suggest that all of the consensus proteins adopt their archetypal fold. Support for folding is provided by the observation that all consensus proteins tested show their expected biological activities (Figures 2, 4, and 5).

Our findings indicate that thermodynamic stabilization of consensus proteins is the norm, rather than the exception. Four of the six (and five of the seven including the previously reported homeodomain (30)) consensus proteins showed stabilities greater than the most stable naturally-occurring sequences identified in our literature search, and the other two showed stabilities near and above average (Figure 3; Table S3). In short, consensus design can be expected to provide stability enhancements about three quarters of the time. This result is particularly surprising, given that proteins are not under direct evolutionary selection for maximal stability (49, 50), but must simply retain sufficient stability to remain folded. It appears that by taking the most probable residue at each position, a large number of small stability enhancements sum to a large net increase in stability. Although naturally occurring extant proteins are of lower stability (perhaps because high stabilities are not required for function) this information gets

encoded in alignments of large numbers of sequences. Taken at face value, these results highlight the importance of information encoded at the level of single residues. Though single-residue information does not explicitly include pairwise sequence correlations, favorable pairs may be retained in our consensus designs as long as each residue in the pair is highly conserved. Thus, the extent to which consensus sequences capture such "accidental" correlations and their contributions to the observed effects on stability require further studies.

The source of the relative instability stability of consensus SH3 is unclear. The consensus SH3 and the extant sequences from which it was generated have some exceptional features, although none of these are unique to SH3. The SH3 sequences are among the shortest sequence families examined (54 residues) although not the shortest (NTL9 is 46 residues). The consensus SH3 sequences has a high fraction of polar residues and the lowest fraction of uncharged residues (Figure 6A), although the consensus homeodomain is a close second. The SH3 sequence is also the only protein in our set that has an all-β structure.

Taxonomically, sequences in the SH3 MSA show the lowest pairwise identity (26%, Table S1), although the SH2 family is a close second (28%). It may be noteworthy that the increase in stability of consensus SH2 compared to the available extant values is the smallest stability increment observed for those proteins likely to conform to a two-state mechanism. It may also be noteworthy that along with SH2, the SH3 multiple sequence is uniquely dominated by eukaryotic sequences. In a study of consensus superoxide dismutase sequences, Goyal and Magliery found successful

consensus design to be highly dependent on the phylogeny represented in the MSA (51). Stabilities in consensus RNaseH sequences in the Marqusee group show also show a strong phylogenetic dependence in which very broad phylogenetic distribution leads to lower stability and folding cooperativity (S. Marqusee, S. Lim, and C. Nixon, personal communication).

A particular advantage of consensus sequence design is that it draws upon the natural evolutionary history of a protein family. As a result, residues important for function are likely to be conserved (52). However, it cannot be assumed *a priori* that the resulting consensus proteins will show biological function, since consensus sequences are novel sequences that have experienced no evolutionary selection for function. Importantly, all consensus proteins we assayed for function maintained some level of expected biological activities of both molecular recognition and enzymatic catalysis (Figures 4 and 5). This result, combined with previously reported studies showing consensus protein function (20–29), indicates that information necessary for protein function is retained in averaging over many sequences that each individually contain functionally important information.

In both this study and our previous investigations of a consensus homeodomain (30), consensus substitution showed varying effects on molecular recognition. Consensus HD and SH3 each showed 2-3 orders of magnitude differences in their binding affinities to cognate substrates relative to naturally-occurring sequences, with consensus HD showing higher affinity and consensus SH3 showing lower affinity. The origins of these differences in substrate binding affinities remain unclear. It is possible

that the sequences used to obtain the consensus homeodomain sequence bind similar sequences (indeed, many of these sequences are from the engrailed superfamily), resulting in an “optimized” homeodomain, whereas sequences used to obtain the consensus SH3 possess different specificities, resulting in a sequence whose binding affinity has been “averaged out.” Testing this explanation will require an investigation of the binding specificities of the consensus proteins as well as those of the sequences used to generate them.

For the three enzymes examined here, consensus substitution shows fairly consistent effects on catalysis. Steady-state turnover rates, determined at 20 °C, for all consensus enzymes were lower than those for naturally-occurring mesophilic sequences, but on par with those of thermophilic sequences at similiar temperatures (Table 2). This is consistent with the observation that thermophilic proteins show lower catalytic activities at low temperatures than their less stable mesophilic counterparts (53, 54), an observation that has widely been interpreted as resulting from a trade-off between dynamics and catalysis (55). As this issue is still debated (56, 57), consensus sequence design may offer a promising avenue to gain insights into the relationships among protein stability, dynamics, activity, and evolution.

The consensus design strategy used here appears to impart strong sequence biases, that is, taking the most probable residue at each position does not result in average sequence statistics. These biases may have significant effects on stability and function. The consensus sequences all have a high content of charged residues and low content of polar noncharged residues (Figure 6). Such sequence biases have also

been observed, albeit potentially to a lesser degree, in thermophilic sequences (58), consistent with the high stabilities observed for the consensus proteins. Makhatadze et al have been able to increase stability by introducing charged residues at surface positions of several proteins and optimizing electrostatic interactions (59, 60). It is unclear to what extent the locations of consensus charged residues optimize electrostatic interactions, or whether additional stability increases can be obtained by charge shuffling. Increases in stability and solubility have also been reported for "supercharged" proteins, which have similar numbers of charged residues (61), however, the consensus proteins studied here are generally close electroneutrality, whereas supercharged proteins have highly imbalanced positive or negative charge.

It should be noted, however, that some of the consensus sequences deviate from the general trends observed in sequence biases. For instance, consensus SH3 and HD have a greater percentage of polar residues and a lower percentage of nonpolar residues, and consensus DHFR has a much lower net charge, compared to the average for each MSA. Thus, consensus sequence statistics appear to abide by general trends but not absolute rules.

Similarly, analysis of the positions at which the consensus sequences differ from extant sequences highlight important aspects about the consensus design strategy. These consensus mismatches occur mainly at positions with relatively low conservation and positions on the protein surface (Figure 6), consistent with the well-known correlation between residue conservation and solvent accessible surface area (62). This may highlight an implicit advantage of consensus sequence design, since substitutions

at core positions are often destabilizing (63). However, the large observed effects of consensus substitution on both stability and activity indicate that these weakly conserved and surface positions play a sizable role in both stability and function, and considerable gains can be made by optimizing these positions. This observation is consistent with the observation of the functional impacts of nonconserved "rheostat" substitutions on the surface of lac repressor (64). Furthermore, the importance of these weakly conserved positions suggests that using a large number of sequences may a key component of successful consensus design, since weakly conserved positions are most sensitive to phylogenetic noise and misalignment (65).

Our work here demonstrates that the consensus sequence design method is both a general and successful strategy to design proteins of high stability that retain biological activity. Compared to other rational, structure-based, or directed evolution methods, consensus sequence design provides a simple route to accomplish longstanding goals of protein design. Furthermore, its foundation in phylogenetics provides a promising avenue to address questions regarding the relationships of protein sequence, biophysics, and evolution.

Materials and Methods

Design of consensus sequences

Sequences for each family were gathered from Pfam (31), SMART (32), or InterPro (33) databases. Resulting sequence sets for each domain were filtered by sequence length, removing sequences 30% longer or shorter than the median

sequence length of the set. To avoid bias from sequence groups with high identity, we used CD-HIT (66) to cluster sequences at 90% identity and selected a single representative sequence from each cluster. This curated sequence set was used to generate a multiple sequence alignment using MAFFT (67).

At each position of the multiple sequence alignment, frequencies were determined for the 20 amino acids along with a gap frequency using an in-house script. Positions occupied by residues (as opposed to a gap) in at least half of the sequences were included as positions in the consensus sequence. The most frequent residue at each of these "consensus positions" was gathered to create the consensus sequence for that protein family.

NMR spectroscopy

^{15}N- and ^{13}C,^{15}N-isotopically labeled proteins were expressed in *E. coli* BL21(DE3) cells grown in M9 minimal media supplemented with $^{15}NH_4Cl$ and either ^{12}C- or ^{13}C-glucose (Cambridge Isotope Laboratories). Proteins were purified as described in the Supplementary Methods, and were concentrated to 400-800 μM for NMR spectroscopy.

^{1}H-^{15}N HSQC spectra were collected for ^{15}N-labeled consensus NTL9, SH3, HD, SH2, DHFR, and AK at 25 °C on Bruker Avance or Avance II 600 MHz spectrometers equipped with cryoprobes. NMR samples for NTL9, SH3, HD, and SH2 contained 150 mM NaCl, 5% D_2O, and 25 mM $NaPO_4$ (pH 7.0). Spectra of consensus DHFR were collected under the same conditions both without and with a 1:1 molar equivalent of

methotrexate (Sigma Aldrich). Spectra of consensus AK were collected in 50 mM NaCl, 1 mM TCEP, 5% D_2O, and 25 mM Tris-HCl (pH 7.5) at 25 °C. For ^{15}N-labeled consensus PGK, ^{1}H-^{15}N TROSY spectra were collected on a Varian 800 MHz spectrometer at 35 °C. NMR samples of consensus PGK contained 50 mM NaCl, 1 mM TCEP, 5% D_2O, and 25 mM Tris-HCl (pH 7.5).

All data were processed and analyzed using NMRPipe (68) and NMRFAM-SPARKY (69). Backbone assignments for consensus NTL9, SH3, and SH2 were made using standard triple-resonance experiments including HNCACB, HNCO, HN(CA)N on Bruker Avance or Avance II 600 MHz spectrometers. Backbone chemical shift data were used for secondary structure predictions using TALOS-N (70).

Peptide binding to consensus SH3 was monitored by heteronuclear NMR spectroscopy. A putative SH3-binding peptide (Ac-PLPPLPRRALSVW-NH_2) was synthesized by GenScript. Samples containing 200 μM ^{15}N-labeled SH3 were prepared at 0-, 0.05-, 0.125-, 0.5-, 1.25-, 2.5-, 5-, 10-, and 20-fold molar equivalents of unlabeled peptide. ^{1}H-^{15}N HSQC spectra were collected on a Bruker Avance 600 MHz spectrometer in 150 mM NaCl, and 5% D_2O, 25 mM $NaPO_4$ (pH 7.0) at 25 °C. ^{1}H-^{15}N chemical shifts varied monotonically with peptide concentrations such that assignments from the apo-protein could be transferred to the bound state. At each peptide concentration, chemical shift perturbations for each residue ($\Delta\delta_{NH,i}$) were calculated as a weighted Pythagorean distance:

$$\Delta\delta_{NH,i}=\sqrt{\frac{1}{2}[\Delta\delta_{H,i}^2 + 0.14\Delta\delta_{N,i}^2]} \quad (1)$$

where $\Delta\delta_{X,i}$ is the change in chemical shift of the ith resonance in either ^{15}N or ^{1}H, relative to the apo-protein chemical shift value (71). The weighting factor of 0.14 accounts for differences in ^{1}H and ^{15}N chemical shift sensitivities. For the ten peaks showing the greatest changes, chemical shift perturbations at each peptide concentrations were globally fit to the single-site binding equation:

$$\Delta\delta_{NH} = \Delta\delta_{max} \frac{([P]_t + [L]_t + K_d) - \sqrt{([P]_t + [L]_t + K_d)^2 - 4[P]_t[L]_t}}{2[P]_t} \quad (2)$$

where $\Delta\delta_{max}$ is a local parameter for maximal chemical shift perturbation for each peak, $[P]_t$ is the total consensus SH3 concentration, $[L]_t$ is the total peptide concentration, and K_d is a global dissociation constant (71). In the fit, $\Delta\delta_{max}$ values were optimized locally (for each of the ten resonances), K_d was optimized globally, and $[P]_t$ was fixed at its known value.

Circular dichroism and fluorescence spectroscopies

Circular dichroism measurements were collected on an Aviv Model 435 CD spectropolarimeter. Far-UV CD spectra were collected using a 1 mm cuvette with protein concentrations ranging from 2-31 μM at 20 °C, averaging for 5 s with a 1 nm step size. Consensus NTL9, SH3, HD, SH2, and DHFR were collected in 150 mM NaCl and 25 mM $NaPO_4$ (pH 7.0). Consensus AK and PGK were collected in 50 mM NaCl, 0.5 mM TCEP, and 25 mM Tris-HCl (pH 8.0).

Guanidine hydrochloride (GdnHCl)-induced folding/unfolding transitions were monitored using either CD or fluorescence spectroscopy. All unfolding transitions were collected at 20 °C with protein concentrations ranging from 1-6 μM. UltraPure GdnHCl

was purchased from Invitrogen. Concentrations of GdnHCl were verified using refractometry (72). Folding/unfolding equilibration was verified for all proteins by either superposition of titrations obtained by adding GdnHCl with titrations obtained by diluting GdnHCl, or by determining the time for complete relaxation after a rapid jump to the midpoint GdnHCl concentration, and allowing for at least 5 half-times equilibration prior to measurement.

Unfolding of consensus DHFR was monitored by CD at 222 nm, signal averaging for 30 s at each guanidine concentration. Unfolding of consensus NTL9, SH3, and SH2 was monitored by tryptophan fluorescence on an Aviv Model 107 ATF. Fluorescence was measured using a 280 nm excitation and either a 332 nm (SH2 and SH3) or 348 nm (NTL9) emission. For these four proteins, unfolding was found to equilibrate rapidly, so that titrations could be generated using a Hamilton automated titrator, with a 5 minute equilibration period. Fluorescence emission was averaged over 30 seconds.

Folding/unfolding of consensus AK and PGK was found to equilibrate on a slower timescale than the other consensus proteins, prohibiting the use of an automated titrator. Therefore, samples at each denaturant concentration were made individually and equilibrated at room temperature for 24 hours (AK) or 5 hours (PGK). For each sample, the CD signal at 225 nm (AK) or 222 nm (PGK) was averaged for 30 s. Melts for both proteins were collected in buffer containing, 50 mM NaCl, 0.5 mM TCEP, and 25 mM Tris-HCl (pH 8.0).

Titrations were carried out in triplicate for each protein. Thermodynamic folding/unfolding parameters were determined by fitting a two-state linear extrapolation model to the folding/unfolding curves (73).

Steady-state enzyme kinetics

Steady-state enzyme kinetic parameters were determined for consensus DHFR, AK, and PGK using absorbance spectroscopy to monitor the oxidation of NAD(P)H catalyzed either directly by the consensus enzyme (DHFR; (74)), or by the activity of an enzyme that is directly coupled to the products produced by the rate-limiting activity of the consensus enzyme (AK and PGK; (54, 75)). The absorbance at 340 nm was monitored over time after rapid addition of consensus enzyme. Steady-state velocities were determined as the initial linear slope of the time course. Because all studied consensus enzymes catalyze bi-substrate reactions, Michealis-Menten kinetics were obtained by varying the concentration of one substrate at a constant, saturating concentration of the other substrate.

For DHFR assays, a concentration of 175 nM consensus DHFR was used in reaction buffer containing 25 mM HEPES (pH 7.5), 150 mM NaCl, and either 150 mM NADPH (for reactions where DHF was varied) or 100 mM DHF (for reactions where NADPH was varied). For AK assays, a concentration of 53 nM consensus AK was used in reaction buffer containing 50 mM HEPES (pH 7.5), 100 mM NaCl, 20 mM $MgCl_2$, 1 mM phosphoenolpyruvate, 0.1 mM NADH, 10 units pyruvate kinase, 10 units lactate dehydrogenase, and 5 mM AMP. For PGK assays, a concentration of 53 nM consensus

PGK was used in reaction mixture containing 100 mM Tris-HCl (pH 8.0), 3 mM $MgCl_2$, 0.1 mM NADH, 5 units glyceraldehyde phosphate dehydrogenase, and either 20 mM ATP or 10 mM 3-PG at pH 8.0. All assays were performed at 20 °C. A Michaelis-Menten model was fit to the data to obtain k_{cat} and K_m for the varied substrate in each titration.

Acknowledgements

The authors thank Ananya Majumdar and the Johns Hopkins University Biomolecular NMR Center, and the Center for Molecular Biophysics for providing facilities and resources. This work was supported by National Institutes of Health grant GM068462 to DB. MS was supported by NIH grants T32GM008403 and F31GM128295.

References

1. Gagner JE, Kim W, Chaikof EL (2014) Designing protein-based biomaterials for medical applications. *Acta Biomater* 10(4):1542–1557.

2. Jemli S, Ayadi-Zouari D, Hlima HB, Bejar S (2016) Biocatalysts: application and engineering for industrial purposes. *Crit Rev Biotechnol* 36(2):246–258.

3. Khoury GA, Smadbeck J, Kieslich CA, Floudas CA (2014) Protein folding and de novo protein design for biotechnological applications. *Trends Biotechnol* 32(2):99–109.

4. Rothlisberger D, et al. (2008) Kemp elimination catalysts by computational enzyme design. *Nature* 453(7192):190–195.

5. Kulshreshtha S, Chaudhary V, Goswami GK, Mathur N (2016) Computational approaches for predicting mutant protein stability. *J Comput Aided Mol Des* 30(5):401–412.

6. Chen C-Y, Georgiev I, Anderson AC, Donald BR (2009) Computational structure-based redesign of enzyme activity. *Proc Natl Acad Sci U S A* 106(10):3764–3769.

7. Jackel C, Kast P, Hilvert D (2008) Protein design by directed evolution. *Annu Rev Biophys* 37:153–173.

8. Kries H, Blomberg R, Hilvert D (2013) De novo enzymes by computational design. *Curr Opin Chem Biol* 17(2):221–228.

9. Li Z, Yang Y, Zhan J, Dai L, Zhou Y (2013) Energy functions in de novo protein design: current challenges and future prospects. *Annu Rev Biophys* 42:315–335.

10. Gainza P, Nisonoff HM, Donald BR (2016) Algorithms for protein design. *Curr Opin Struct Biol* 39:16–26.

11. Lane MD, Seelig B (2014) Advances in the directed evolution of proteins. *Curr Opin Chem Biol* 22:129–136.

12. Porebski BT, Buckle AM (2016) Consensus protein design. *Protein Eng Des Sel PEDS* 29(7):245–251.

13. Steipe B, Schiller B, Pluckthun A, Steinbacher S (1994) Sequence statistics reliably predict stabilizing mutations in a protein domain. *J Mol Biol* 240(3):188–192.

14. Sullivan BJ, et al. (2012) Stabilizing Proteins from Sequence Statistics: The Interplay of Conservation and Correlation in Triosephosphate Isomerase Stability. *J Mol Biol* 420(4–5):384–399.

15. Polizzi KM, Chaparro-Riggers JF, Vazquez-Figueroa E, Bommarius AS (2006) Structure-guided consensus approach to create a more thermostable penicillin G acylase. *Biotechnol J* 1(5):531–536.

16. Rath A, Davidson AR (2000) The design of a hyperstable mutant of the Abp1p SH3 domain by sequence alignment analysis. *Protein Sci Publ Protein Soc* 9(12):2457–2469.

17. Nikolova PV, Henckel J, Lane DP, Fersht AR (1998) Semirational design of active tumor suppressor p53 DNA binding domain with enhanced stability. *Proc Natl Acad Sci U S A* 95(25):14675–14680.

18. Giver L, Gershenson A, Freskgard PO, Arnold FH (1998) Directed evolution of a thermostable esterase. *Proc Natl Acad Sci U S A* 95(22):12809–12813.

19. Zhao H, Arnold FH (1999) Directed evolution converts subtilisin E into a functional equivalent of thermitase. *Protein Eng* 12(1):47–53.

20. Desjarlais JR, Berg JM (1993) Use of a zinc-finger consensus sequence framework and specificity rules to design specific DNA binding proteins. *Proc Natl Acad Sci U S A* 90(6):2256–2260.

21. Lehmann M, et al. (2002) The consensus concept for thermostability engineering of proteins: further proof of concept. *Protein Eng* 15(5):403–411.

22. Sullivan BJ, Durani V, Magliery TJ (2011) Triosephosphate isomerase by consensus design: dramatic differences in physical properties and activity of related variants. *J Mol Biol* 413(1):195–208.

23. Porebski BT, et al. (2016) Smoothing a rugged protein folding landscape by sequence-based redesign. *Sci Rep* 6:33958.

24. Porebski BT, et al. (2016) Circumventing the stability-function trade-off in an engineered FN3 domain. *Protein Eng Des Sel PEDS*. doi:10.1093/protein/gzw046.

25. Stevens AJ, et al. (2016) Design of a Split Intein with Exceptional Protein Splicing Activity. *J Am Chem Soc* 138(7):2162–2165.

26. Aerts D, et al. (2013) Consensus engineering of sucrose phosphorylase: the outcome reflects the sequence input. *Biotechnol Bioeng* 110(10):2563–2572.

27. Blatt LM, Davis JM, Klein SB, Taylor MW (1996) The biologic activity and molecular characterization of a novel synthetic interferon-alpha species, consensus interferon. *J Interferon Cytokine Res Off J Int Soc Interferon Cytokine Res* 16(7):489–499.

28. Garcia-Guevara F, Bravo I, Martinez-Anaya C, Segovia L (2017) Cofactor specificity switch in Shikimate dehydrogenase by rational design and consensus engineering. *Protein Eng Des Sel PEDS* 30(8):533–541.

29. Huang L, et al. (2012) The design and recombinant protein expression of a consensus porcine interferon: CoPoIFN-alpha. *Cytokine* 57(1):37–45.

30. Tripp KW, Sternke M, Majumdar A, Barrick D (2017) Creating a Homeodomain with High Stability and DNA Binding Affinity by Sequence Averaging. *J Am Chem Soc*. doi:10.1021/jacs.6b11323.

31. Bateman A, et al. (2004) The Pfam protein families database. *Nucleic Acids Res* 32.

32. Letunic I, Doerks T, Bork P (2015) SMART: recent updates, new developments and status in 2015. *Nucleic Acids Res* 43(Database issue):D257-260.

33. Finn RD, et al. (2017) InterPro in 2017-beyond protein family and domain annotations. *Nucleic Acids Res* 45(D1):D190–D199.

34. Fukami-Kobayashi K, Nosaka M, Nakazawa A, Go M (1996) Ancient divergence of long and short isoforms of adenylate kinase: molecular evolution of the nucleoside monophosphate kinase family. *FEBS Lett* 385(3):214–220.

35. Viguera AR, Martinez JC, Filimonov VV, Mateo PL, Serrano L (1994) Thermodynamic and kinetic analysis of the SH3 domain of spectrin shows a two-state folding transition. *Biochemistry* 33(8):2142–2150.

36. Loveridge EJ, et al. (2011) The role of large-scale motions in catalysis by dihydrofolate reductase. *J Am Chem Soc* 133(50):20561–20570.

37. Myers JK, Pace CN, Scholtz JM (1995) Denaturant m values and heat capacity changes: relation to changes in accessible surface areas of protein unfolding. *Protein Sci Publ Protein Soc* 4(10):2138–2148.

38. Geierhaas CD, Nickson AA, Lindorff-Larsen K, Clarke J, Vendruscolo M (2007) BPPred: a Web-based computational tool for predicting biophysical parameters of proteins. *Protein Sci Publ Protein Soc* 16(1):125–134.

39. Demers J-P, Mittermaier A (2009) Binding mechanism of an SH3 domain studied by NMR and ITC. *J Am Chem Soc* 131(12):4355–4367.

40. Saksela K, Permi P (2012) SH3 domain ligand binding: What's the consensus and where's the specificity? *FEBS Lett* 586(17):2609–2614.

41. Shenkin PS, Erman B, Mastrandrea LD (1991) Information-theoretical entropy as a measure of sequence variability. *Proteins* 11(4):297–313.

42. Reidhaar-Olson JF, Sauer RT (1988) Combinatorial cassette mutagenesis as a probe of the informational content of protein sequences. *Science* 241(4861):53–57.

43. Rennell D, Bouvier SE, Hardy LW, Poteete AR (1991) Systematic mutation of bacteriophage T4 lysozyme. *J Mol Biol* 222(1):67–88.

44. Mosavi LK, Minor DLJ, Peng Z-Y (2002) Consensus-derived structural determinants of the ankyrin repeat motif. *Proc Natl Acad Sci U S A* 99(25):16029–16034.

45. Aksel T, Majumdar A, Barrick D (2011) The contribution of entropy, enthalpy, and hydrophobic desolvation to cooperativity in repeat-protein folding. *Struct Lond Engl 1993* 19(3):349–360.

46. Main ERG, Xiong Y, Cocco MJ, D'Andrea L, Regan L (2003) Design of stable alpha-helical arrays from an idealized TPR motif. *Struct Lond Engl 1993* 11(5):497–508.

47. Parmeggiani F, et al. (2008) Designed armadillo repeat proteins as general peptide-binding scaffolds: consensus design and computational optimization of the hydrophobic core. *J Mol Biol* 376(5):1282–1304.

48. Socolich M, et al. (2005) Evolutionary information for specifying a protein fold. *Nature* 437(7058):512–518.

49. Taverna DM, Goldstein RA (2002) Why are proteins marginally stable? *Proteins* 46(1):105–109.

50. Bloom JD, Raval A, Wilke CO (2007) Thermodynamics of neutral protein evolution. *Genetics* 175(1):255–266.

51. Goyal VD, Magliery TJ (2018) Phylogenetic Spread of Sequence Data Affects Fitness of SOD1 Consensus Enzymes: Insights from Sequence Statistics and Structural Analyses. *Proteins*. doi:10.1002/prot.25486.

52. Capra JA, Singh M (2007) Predicting functionally important residues from sequence conservation. *Bioinforma Oxf Engl* 23(15):1875–1882.

53. Holland LZ, McFall-Ngai M, Somero GN (1997) Evolution of lactate dehydrogenase-A homologs of barracuda fishes (genus Sphyraena) from different thermal environments: differences in kinetic properties and thermal stability are due to amino acid substitutions outside the active site. *Biochemistry* 36(11):3207–3215.

54. Wolf-Watz M, et al. (2004) Linkage between dynamics and catalysis in a thermophilic-mesophilic enzyme pair. *Nat Struct Mol Biol* 11(10):945–949.

55. Varley PG, Pain RH (1991) Relation between stability, dynamics and enzyme activity in 3-phosphoglycerate kinases from yeast and Thermus thermophilus. *J Mol Biol* 220(2):531–538.

56. Studer RA, Christin P-A, Williams MA, Orengo CA (2014) Stability-activity tradeoffs constrain the adaptive evolution of RubisCO. *Proc Natl Acad Sci U S A* 111(6):2223–2228.

57. Tian J, Woodard JC, Whitney A, Shakhnovich EI (2015) Thermal stabilization of dihydrofolate reductase using monte carlo unfolding simulations and its functional consequences. *PLoS Comput Biol* 11(4):e1004207.

58. Kumar S, Tsai CJ, Nussinov R (2000) Factors enhancing protein thermostability. *Protein Eng* 13(3):179–191.

59. Strickler SS, et al. (2006) Protein stability and surface electrostatics: a charged relationship. *Biochemistry* 45(9):2761–2766.

60. Gribenko AV, et al. (2009) Rational stabilization of enzymes by computational redesign of surface charge-charge interactions. *Proc Natl Acad Sci U S A* 106(8):2601–2606.

61. Lawrence MS, Phillips KJ, Liu DR (2007) Supercharging proteins can impart unusual resilience. *J Am Chem Soc* 129(33):10110–10112.

62. Koshi JM, Goldstein RA (1997) Mutation matrices and physical-chemical properties: correlations and implications. *Proteins* 27(3):336–344.

63. Tokuriki N, Stricher F, Schymkowitz J, Serrano L, Tawfik DS (2007) The stability effects of protein mutations appear to be universally distributed. *J Mol Biol* 369(5):1318–1332.

64. Meinhardt S, Manley MWJ, Parente DJ, Swint-Kruse L (2013) Rheostats and toggle switches for modulating protein function. *PloS One* 8(12):e83502.

65. Talavera G, Castresana J (2007) Improvement of phylogenies after removing divergent and ambiguously aligned blocks from protein sequence alignments. *Syst Biol* 56(4):564–577.

66. Li W, Jaroszewski L, Godzik A (2001) Clustering of highly homologous sequences to reduce the size of large protein databases. *Bioinforma Oxf Engl* 17(3):282–283.

67. Katoh K, Misawa K, Kuma K, Miyata T (2002) MAFFT: a novel method for rapid multiple sequence alignment based on fast Fourier transform. *Nucleic Acids Res* 30(14):3059–3066.

68. Delaglio F, et al. (1995) NMRPipe: a multidimensional spectral processing system based on UNIX pipes. *J Biomol NMR* 6(3):277–293.

69. Lee W, Tonelli M, Markley JL (2015) NMRFAM-SPARKY: enhanced software for biomolecular NMR spectroscopy. *Bioinforma Oxf Engl* 31(8):1325–1327.

70. Shen Y, Bax A (2015) Protein structural information derived from NMR chemical shift with the neural network program TALOS-N. *Methods Mol Biol Clifton NJ* 1260:17–32.

71. Williamson MP (2013) Using chemical shift perturbation to characterise ligand binding. *Prog Nucl Magn Reson Spectrosc* 73:1–16.

72. Nozaki Y (1972) The preparation of guanidine hydrochloride. *Methods Enzymol* 26:43–50.

73. Pace CN (1986) Determination and analysis of urea and guanidine hydrochloride denaturation curves. *Methods Enzymol* 131:266–280.

74. Bhabha G, et al. (2013) Divergent evolution of protein conformational dynamics in dihydrofolate reductase. *Nat Struct Mol Biol* 20(11):1243–1249.

75. Bentahir M, et al. (2000) Structural, kinetic, and calorimetric characterization of the cold-active phosphoglycerate kinase from the antarctic Pseudomonas sp. TACII18. *J Biol Chem* 275(15):11147–11153.

76. Fierke CA, Johnson KA, Benkovic SJ (1987) Construction and evaluation of the kinetic scheme associated with dihydrofolate reductase from Escherichia coli. *Biochemistry* 26(13):4085–4092.

77. Kim HS, Damo SM, Lee S-Y, Wemmer D, Klinman JP (2005) Structure and hydride transfer mechanism of a moderate thermophilic dihydrofolate reductase from Bacillus stearothermophilus and comparison to its mesophilic and hyperthermophilic homologues. *Biochemistry* 44(34):11428–11439.

78. Aviram HY, et al. (2018) Direct observation of ultrafast large-scale dynamics of an enzyme under turnover conditions. *Proc Natl Acad Sci U S A*. doi:10.1073/pnas.1720448115.

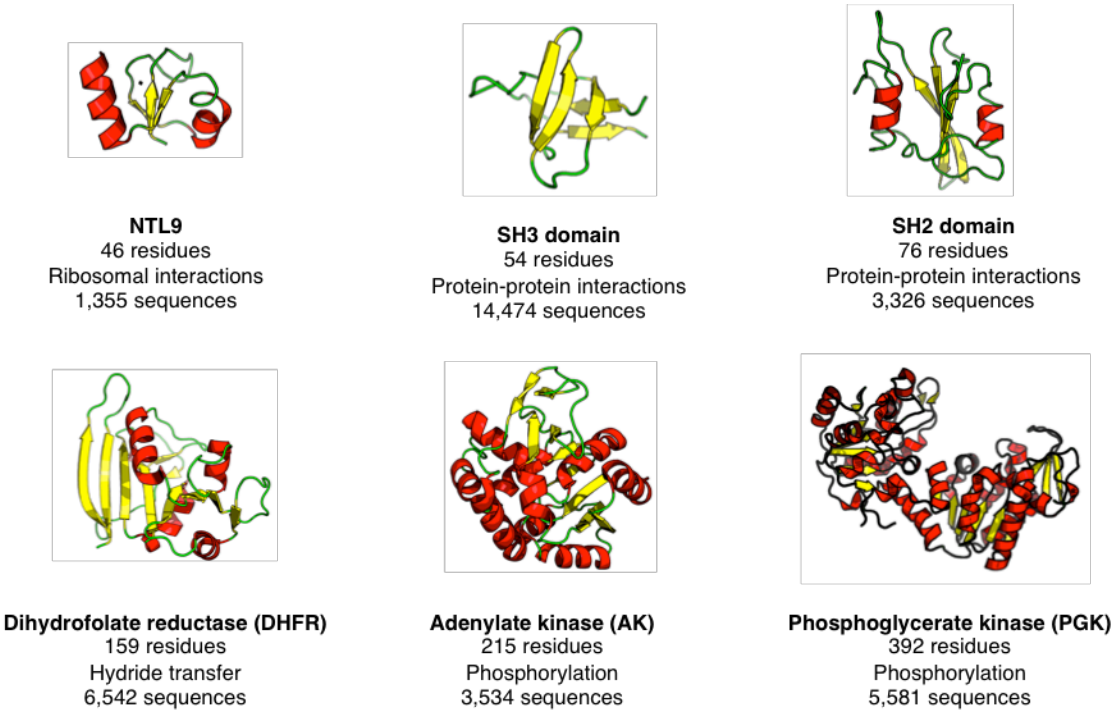

Figure 1. Targets for consensus design. A representative structure of an extant sequence is shown for each target family (NTL9: 1HBB, SH3: 1LKK, SH2: 4U1P, DHFR: 5DFR, AK: 1ANK, PGK: 1PHP). Length of consensus sequence, biological function, and number of sequences used in final multiple sequence alignment are noted.

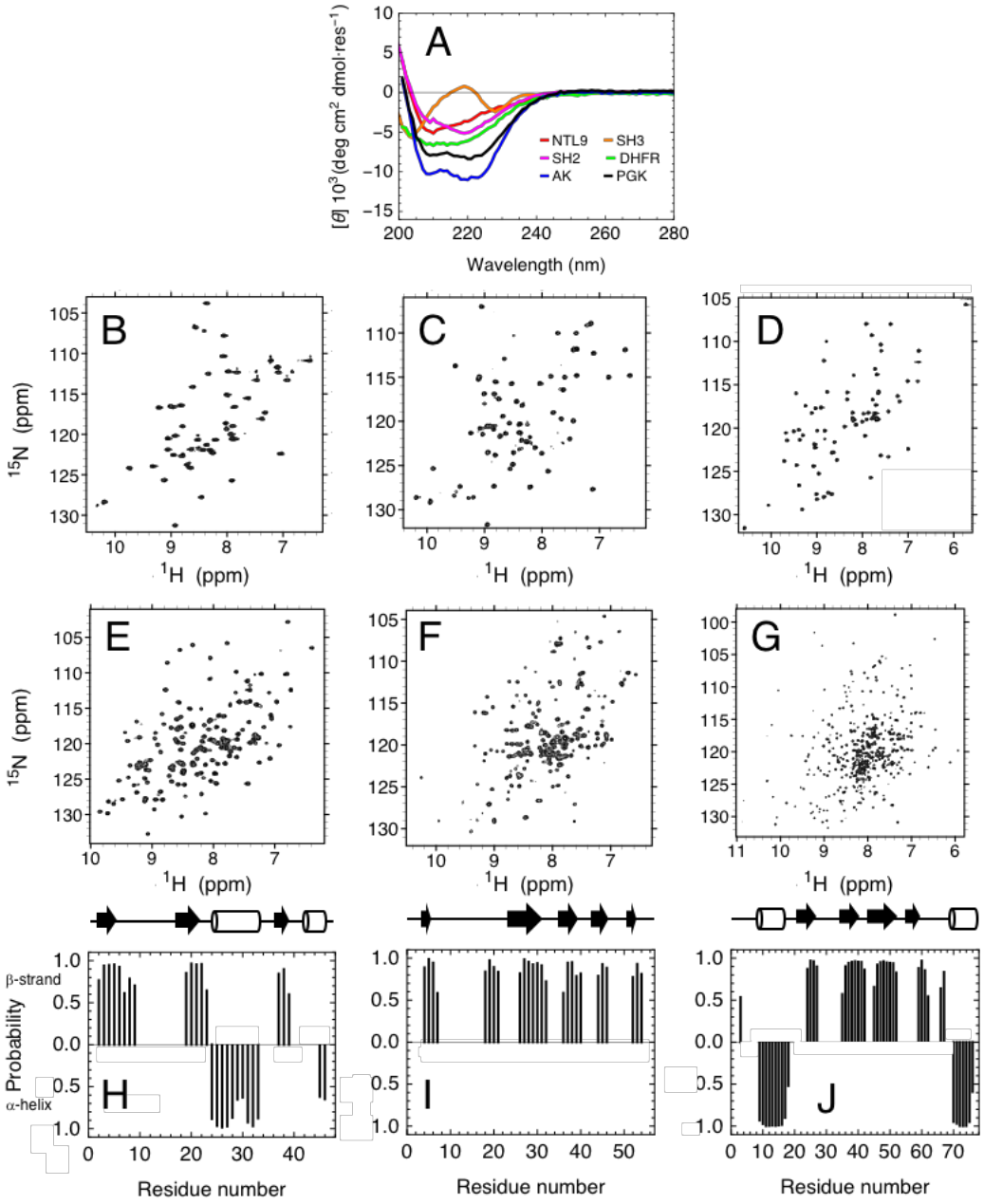

Figure 2. Structural features of consensus proteins. (A) Far-UV CD spectra for all consensus proteins. (B-F) ^{1}H-^{15}N HSQC spectra for consensus (B) NTL9, (C) SH3, (D) SH2, (E) DHFR with addition of 1:1 molar equivalents of methotrexate, and (F) AK at 600 MHz. (G) ^{1}H-^{15}N TROSY spectrum for consensus PGK at 800 MHz. (H-J) Secondary chemical shift-based secondary structure probabilities using backbone resonances calculated by TALOS-N for consensus (H) NTL9, (I) SH3, and (J) SH2.

Schematics above plots represent sequence positions of secondary structures in homology models of consensus sequences.

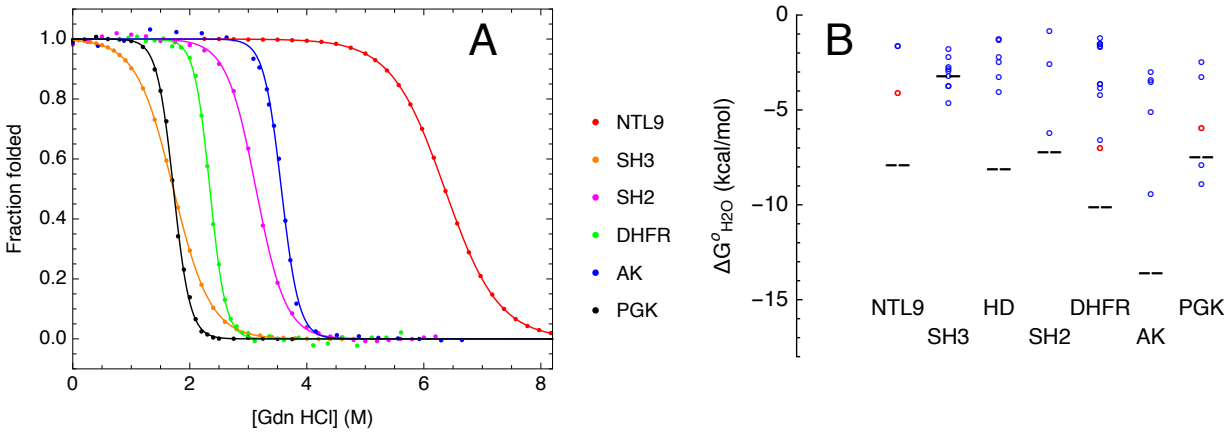

Figure 3. Equilibrium folding of consensus proteins. (A) Representative guanidine hydrochloride-induced folding/unfolding curves for consensus proteins. Data were collected using circular dichroism (DHFR, ADK, PGK) or fluorescence (NTL9, SH3, SH2) spectroscopies. Solid lines are obtained from fitting a two-state model to the data. (B) Comparison of measured folding free energies of consensus proteins to those of extant sequences. Open circles represent folding free energies of extant eukaryotic or mesophilic (blue) and thermophilic (red) sequences. Black dashed lines represent measured folding free energies of consensus sequences. Folding free energy values and sources are reported in TableS3.

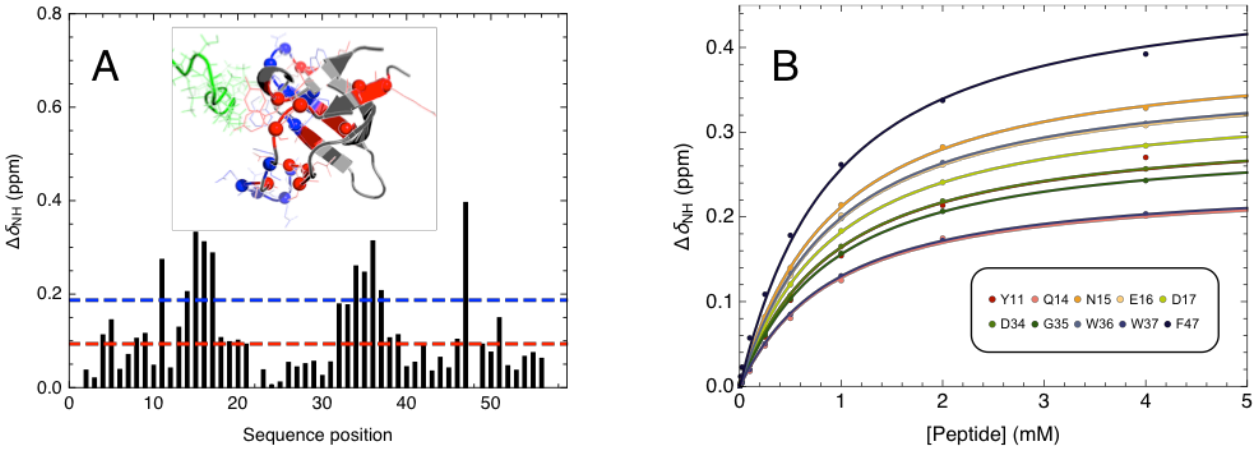

Figure 4. Peptide binding of consensus SH3 by NMR spectroscopy. (A) Chemical shift perturbations (CSPs) of backbone ^{1}H-^{15}N HSQC cross-peaks resulting from addition of a 20-fold excess unlabelled peptide to ^{15}N-labelled consensus SH3. Red and blue lines indicate one and two standard deviations respectively. Inset shows a homology model of consensus SH3 aligned to a peptide-bound structure of human Fyn SH3 (PDB 1A0N; peptide shown in green). Residues showing CSPs greater than one and two standard deviations are shown with alpha carbons as spheres, side chains atoms as lines, and colored red and blue respectively. (B) Binding isotherms for the ten consensus SH3 residues showing largest CSPs. Solid lines are obtained from a global fit to a single-site binding model using a common dissociation constant for all residues.

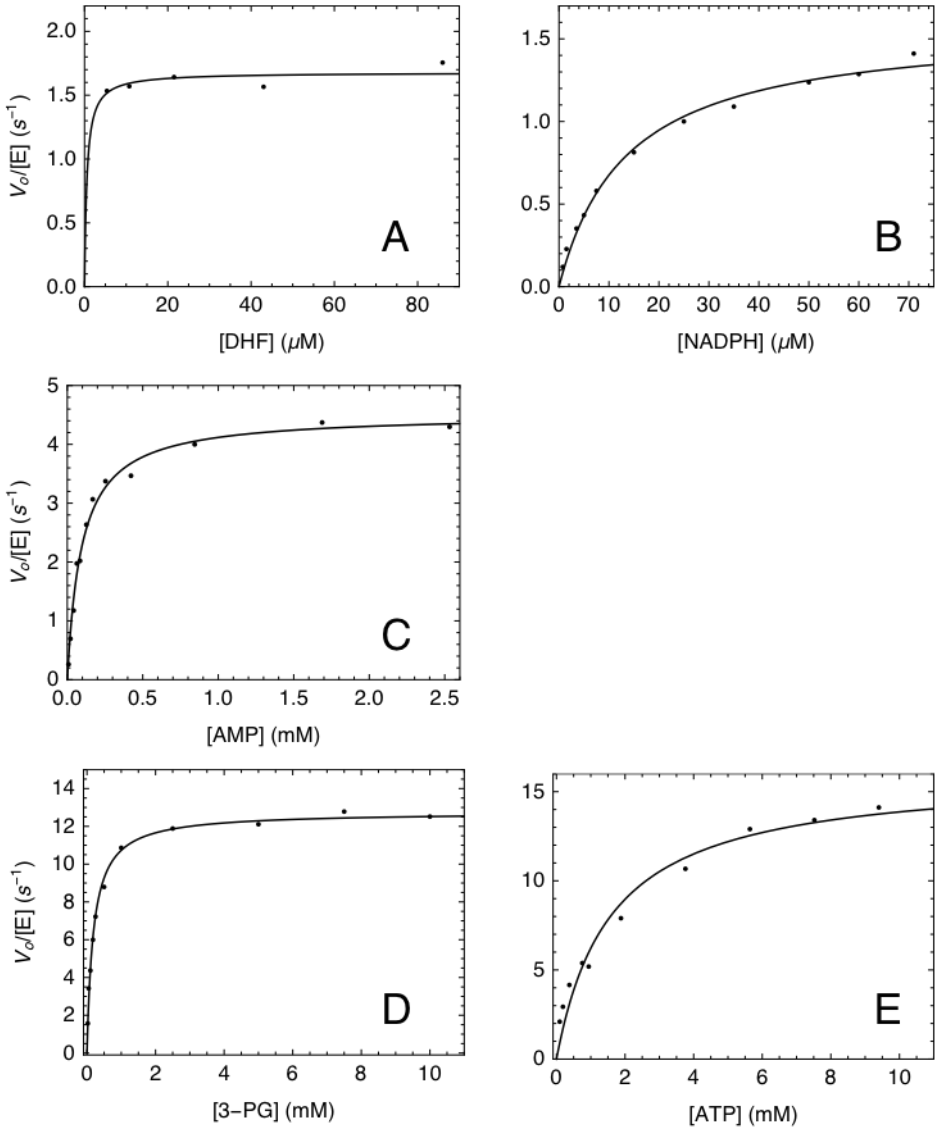

Figure 5. Steady-state kinetics of consensus enzymes. Representative Michaelis-Menten curves generated for each substrate (under saturating conditions of secondary substrate) for consensus DHFR (A: DHF, B: NADPH), ADK (C: AMP), and PGK (D: 3-PG, E: ATP). Solid lines are obtained from fitting a Michaelis-Menten model to the data. In (A), full activity was obtained at the lowest DHF concentration we could measure; as a result, the K_m value for DHF could not be accurately determined.

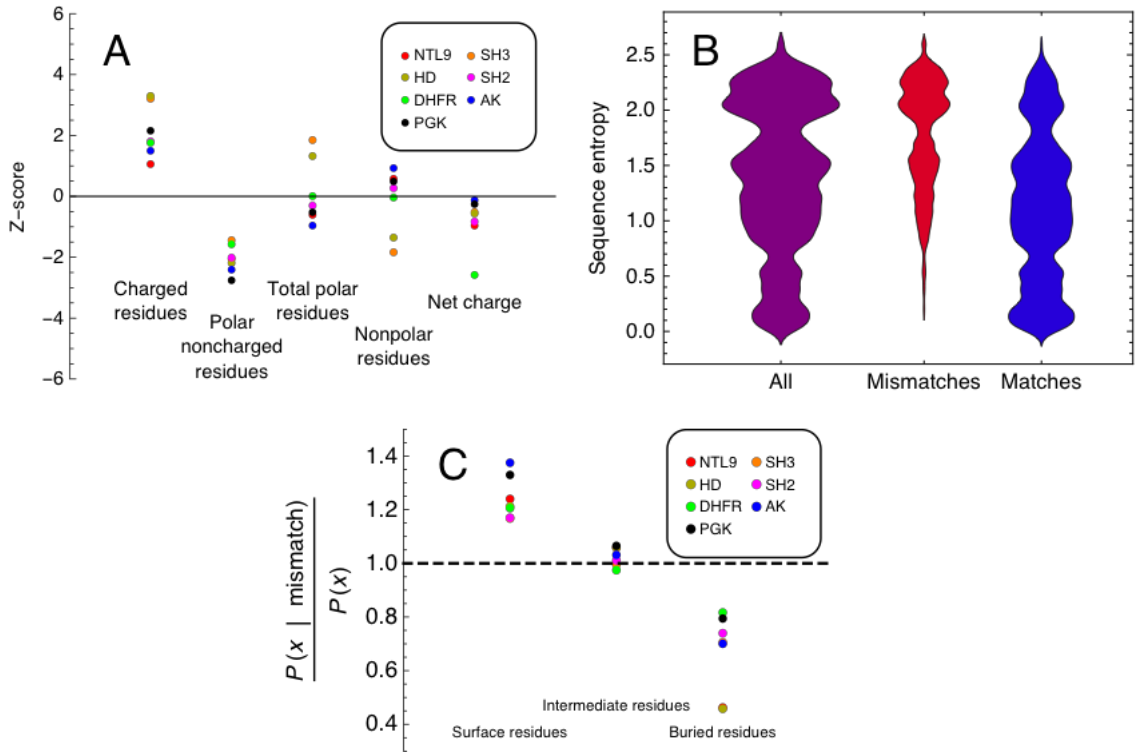

Figure 6. Sequence properties of consensus sequences. (A) Z-scores (the number of standard deviations that separate the consensus sequence from the mean value of sequences in the multiple sequence alignments, equation S1) for various sequence properties. Distributions for all protein families are shown in Figure S9. (B) Distributions of sequence entropy values for all positions in the PGK MSA (purple), positions at which residues in extant sequences differ from the consensus sequence (consensus mismatches; red), and positions at which residues in extant sequences match the consensus sequence (consensus matches; blue) for PGK. Sequence entropy distributions for all protein families are shown in Figure S10. (C) Ratios of conditional probabilities of different structural environments (surface, intermediate, and buried; "X" in the y-label) for consensus mismatches relative to overall probabilities of surface,

intermediate, and buried residues at all positions. Conditional and overall probabilities for all protein families are shown in Figure S11.

Table 1. Equilibrium folding free energies of consensus proteins.

	$\Delta G°_{H2O}$ (kcal mol^{-1})	*m*-value (kcal mol^{-1} M^{-1})	$\Delta\Delta G°_{H2O}$ (kcal mol^{-1})
cNTL9	-7.9 ± 0.1	1.23 ± 0.02	-4.7
cSH3	-3.2 ± 0.1	1.88 ± 0.05	+0.3
cHD	-10.8 ± 0.5	1.60 ± 0.08	-5.3
cSH2	-7.2 ± 0.1	2.28 ± 0.01	-3.6
cDHFR	-10.1 ± 0.1	4.32 ± 0.03	-6.7
cADK	-13.6 ± 0.5	3.83 ± 013	-8.3
cPGK	-7.5 ± 0.2	4.34 ± 0.12	-1.4

$\Delta G°_{H2O}$ and m-values represent the folding free energy extrapolated to water and the denaturant sensitivity of the folding free energy determined from a two-state fit. Reported uncetainties are standard errors of the mean from three independent experiments. $\Delta\Delta G°_{H2O}$ values represent the difference of the measured folding free energy value of the consensus protein and the mean folding free energy value of the naturally-occurring proteins from the literature (see Table S3).

Table 2. Steady-state kinetic parameters of catalysis for consensus and naturally-occurring enzymes.

	Substrate	k_{cat} (s^{-1})	K_m (μM)	k_{cat}/K_m (M^{-1} s^{-1})
Consensus DHFR	DHF	1.7 ± 0.1	< 5 [a]	>3.4 × 10^5
E. coli DHFR[b]		12.3 ± 0.7	0.7 ± 0.2	1.8 ± 0.03 × 10^7
B. stearothermophilus DHFR[c]		2.2	3.5	6.3 × 10^5
Consensus DHFR	NADPH	1.6 ± 0.1	15 ± 2	1.0 ± 0.1 × 10^5
E. coli DHFR[b]		10 ± 1	4.8 ± 1	2.1 ± 0.7 × 10^6
B. stearothermophilus DHFR[c]		2.3	1.5	1.5 × 10^6
Consensus AK	AMP	5.1 ± 0.6	86 ± 10	5.9 ± 1.0 × 10^4
E. coli AK[d]		400 ± 10	120 ± 20	3.3 ± 0.6 × 10^6
A. aeolicus AK[e]		30 ± 10	21	1.4 × 10^6
Consensus PGK	3-PG	12.8 ± 0.1	190 ± 10	6.7 ± 0.3 × 10^4
Yeast PGK[f]		335	590	5.6 × 10^5
T. thermophilus PGK[g]		0.18	NR	NR
Consensus PGK	ATP	14.1 ± 2.1	1200 ± 400	1.2 ± 0.4 × 10^4
Yeast PGK[f]		345	370	4.1 × 10^5
T. thermophilus PGK[g]		0.18	NR	NR

Michaelis-Menten parameters for consensus enzymes (black), a mesophilic enzyme (blue), and a thermophilic enzyme (red). Uncertainties reported for consensus enzymes represent standard errors of the mean from two independent experiments. Experiments for consensus enzymes were performed at 20 °C. NR denotes values that are not reported in the study.

[a]The K_m value for DHF was found to be too low to accurately measure under experimental conditions. Enzyme showed full activity at lowest DHF concentration tested of 5 μM.

[b]Data from reference (76). Experiments were performed at 25 °C.

[c]Data from reference (77). Experiments were performed at 20 °C.

[d]Data from reference (78). Experiments were performed at 25 °C.

[e]Data from reference (54). Experiments were performed at 20 °C.

[f]Data from reference (75). Experiments were performed at 25 °C. Errors were reported to as <5%.

[g]Data from reference (55). Experiments were performed at 25 °C. The reported specific activity of 255 units/mg was converted to turnover rate using a molecular weight of 43 kDa and a 1 mL reaction volume as reported in the study.